

14,01

Micromechanism of plastic deformation enhancement in ultrafine-grained Al-Cu-Zr alloy after annealing and additional deformation

© M.Yu. Gutkin^{1–3}, T.S. Orlova⁴, N.V. Skiba^{4,¶}

¹ Institute for Problems in Mechanical Engineering, Russian Academy of Sciences, St. Petersburg, Russia

² ITMO University, St. Petersburg, Russia

³ Peter the Great Saint-Petersburg Polytechnic University, St. Petersburg, Russia

⁴ Ioffe Institute, St. Petersburg, Russia

¶ E-mail: nikolay.skiba@gmail.com

Received March 24, 2023

Revised March 24, 2023

Accepted March 31, 2023

A theoretical model which describes a micromechanism of plasticity enhancement in an ultrafine-grained Al-Cu-Zr alloy after annealing and additional deformation is suggested. Within the framework of the model, it was shown that nanoprecipitates of the secondary phase Al₂Cu in the grain boundaries become the effective sources of the lattice dislocations in the presence of a large number of the grain boundary dislocations near the nanoprecipitates. The theoretical dependences of the flow stress on the degree of the plastic deformation demonstrate good qualitative and quantitative agreement with the experimental data. The emission of the lattice dislocations from nanoprecipitates provides higher plasticity compared to the emission of the lattice dislocations from the triple junctions of the grain boundaries.

Keywords: ultrafine-grained materials, aluminum alloys, nanoprecipitates, annealing, severe plastic deformation by high-pressure torsion, dislocations, grain boundaries.

DOI: 10.21883/PSS.2023.05.56059.42

1. Introduction

Ultrastrong aluminum alloys are promising for applications as structural and functional materials in various industries, primarily, in automotive, aircraft and electrical engineering industries. Currently, one of the main areas of production of ultrastrong metallic materials with improved strength properties — is formation of nanocrystalline (NC) and ultrafine-grained (UFG) structures by severe plastic deformation (SPD) [1]. Such structures have high grain boundary (GB) density [2–4]. In addition, GBs may be present in them in non-equilibrium state due to extrinsic grain boundary dislocations (EGBDs) and may contain impurity atom segregations and/or second-phase precipitates [4,5]. High GB density as well as specific GB state may significantly improve the strength properties of metals and alloys [2,4]. However, the increase in strength of NC and UFG materials is generally followed by considerable decrease in their ductility [6] resulting in highly limited range of applications of these materials.

At the same time, the experimental results have shown that in certain conditions some multicomponent alloys are able to exhibit unique combination of high strength and good ductility [7–10]. However, not many alloys exhibit such unique mechanical properties. According to the experimental research, the desired combination of high strength and ductility depends on a set of factors, i.e. on

selection of doping elements and combination of additional thermomechanical treatment conditions for alloys. For example, it is well known that copper doping results in grain refinement [11–13] and strengthening [11,14–16] of SPD-treated aluminium alloys.

In particular, a recent research [17] has demonstrated considerable strengthening of Al-Cu-Zr UFG alloy structured by high-pressure torsion (HPT) with good conductivity retained. The authors of [17] have found that, after HPT in this alloy, individual nanoscale precipitates are formed at GBs and contain Cu atoms — Al₂Cu second-phase nanoprecipitates (Al₂Cu NPs) 20–40 nm in size, ellipsoid-shaped, which make considerable contribution to hardening, whose degree is comparable with grain boundary strengthening [17]. Ductility after HPT treatment decreases to 3–5%. However, the next thermomechanical treatment consisting of low-temperature annealing and small additional deformation improves ductility of UFG alloy to a great extent while retaining high level strength [7]. It should be noted that intermediate annealing dramatically reduced ductility of this material to almost brittle state with small strength reduction [7]. It was also shown in [7,18] that nanoscopic precipitates of Al₂Cu in GBs increased in size after annealing (and remained after additional deformation) up to about 60 nm and became faceted, i.e. transformed from ellipsoidal into faceted polyhedral. In this case, it may be reasonably suggested that they acquired edges that

became powerful concentrators of both inherent and applied stresses capable of efficiently emitting lattice dislocations (LDs). NP capability of emitting dislocations is also supported by computer simulations [19,20].

Moreover, SPD is well known to cause the increase in the amount of EGBDs. This was observed in [7], which indicates that, after small additional (after annealing) HPT, dislocation density became 1.8 time higher. Thus, as a result of additional HPT applied to annealed UFG Al-Cu-Zr alloy samples, important structural modifications shall occur in them: 1) GBs shall be enriched with EGBDs, 2) with next loading, gliding EGBDs shall be accumulated near NPs which become effective barriers for EGBD slipping, and 3) under the influence of EGBD pile-ups, these NPs, grown and faceted after annealing, shall become effective sources of LDs which, when emitted into the adjacent grains, shall ensure substantial increase in ductility of UFG alloy.

This study suggests a theoretical model based on assumptions 1) to 3) listed above and aims to explain the experimental findings of [7] that showed increase in ductility of UFG Al-Cu-Zr alloy structured by HPT and then subjected to low-temperature annealing and small additional HPT. For the purpose of this model, LD emission by Al₂Cu NP edges from GBs to adjacent grains is the main plastic deformation mechanism.

2. Model

Consider an individual NP in a GB, simulated by a rectangular inclusion ABCD with dimensions defined by diagonal h and angle α of face BC to the GB plane (Figure 1). It is known [21–25] that plate-like Al₂Cu NPs in copper-oversaturated aluminium-based alloys are formed in such a way that larger faces of Al₂Cu NPs are in {111} planes of the aluminium matrix, and orientation relationships $(110)_{\text{Al}_2\text{Cu}} \parallel (111)_{\text{Al}}$, $[1\bar{1}0]_{\text{Al}_2\text{Cu}} \parallel [10\bar{1}]_{\text{Al}}$ and $[001]_{\text{Al}_2\text{Cu}} \parallel [1\bar{2}1]_{\text{Al}}$ are generally fulfilled on these interfaces. This is explained [25] by a relatively low lattice misfit f at such boundary in orientations $[1\bar{1}0]_{\text{Al}_2\text{Cu}} \parallel [10\bar{1}]_{\text{Al}}$ ($f = 1.23\%$) and $[001]_{\text{Al}_2\text{Cu}} \parallel [1\bar{2}1]_{\text{Al}}$ ($f = 1.71\%$), and by growth kinetics of Al₂Cu intermetallic compound whose faces {110} grow faster than others [21]. It should be noted that recent papers on computer simulation of the structure and properties of such interfaces in lamellar eutectic Al-Al₂Cu composites [23,24] have shown that they relative easily transform from coherent state into semicoherent state due to boundary filling with three families of misfit dislocations (MDs) by means of gliding of Shockley partial dislocations on the boundary. Such interface structure enables it to play a role of a relatively easy interphase slipping plane due to MD movement [23].

For clarity, NP boundaries will be assumed as initially being in coherent state, i.e. containing no MDs. If necessary, this assumption may be omitted, however, as a result the model will be a little sophisticated which will not affect considerably the calculations.

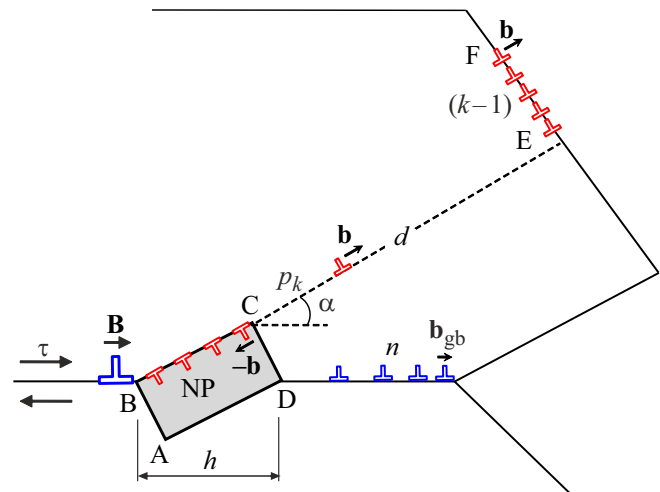


Figure 1. Model of the k -th LD emission from apex C of rectangular NP ABCD and refill of wall EF from $k - 1$ climbing b -dislocations.

Assume hereinafter that the addressed GB contains EGBD pile-ups pressed against NP and GB triple junction. The pile-up in front of NP is simulated by an edge superdislocation with Burgers vector \mathbf{B} (hereinafter B -superdislocation) of magnitude $B = b_{gb}n$, where b_{gb} is the modulus of Burgers vector of an individual EGBD and n is the number of EGBDs in the pile-up.

Within such model, it is reasonable to assume that in the total shear stress field composed of the applied stress τ , the NP stress field and the B -superdislocation stress field, the emission of an LD with Burgers vector \mathbf{b} (hereinafter b -dislocation) from NP apex C into the adjacent grain takes place (Figure 1).

According to the experimental findings and computer simulation of Al₂Cu NPs in aluminium alloys [21–25], the LD easy slip plane will be assumed as coinciding with face plane BC and making angle α with the GB plane. Emission of such b -dislocation may be presented as the origin of a LD dipole with Burgers vectors $\pm\mathbf{b}$ (Figure 1). Consider the mechanism of successive LD emission from the NP edge similar to that suggested before in [26]. The emitted LD will be considered for clarity as positive dislocation of the formed dipole. Within the model developed in [26], the emitted positive LD intersects the grain, achieves the opposite GB and is trapped by it. Then, the next positive LD is emitted that also intersects the grain and is trapped by the opposite GB where the previous LD climbs from the trap point at the GB [26].

As a result of such successive emission of positive LDs and their trapping by the opposite GB, a wall of climbing EGBDs is formed which hinders the next LD emissions by its stress field [26]. Applying this approach to our case, we obtain a defect structure in the form of the k -th LD emitted from the NP edge and wall EF of $k - 1$ climbing b -dislocations (Figure 1).

Within the present model, it is also assumed that negative dislocations ($-b$ -dislocations) of originating LD dipoles slip in the opposite direction from the emission point and form a periodic row along face BC (Figure 1) playing a role of MDs in accordance with the computer simulation data [23,24]. Such MD formation models have been recently studied in relation to composite nanostructures — rectangular cross-section nanowires in nanolayers [27] and in cylindrical nanowires [28]. Forming of such MD row, on the one hand, reduces the NP stress field and increases the total energy gain from LD emission due to reduction of NP strain energy and, on the other hand, reduces total shear stress acting on the emitted LD and, thus, reduces the total energy gain of the system. For the sake of model simplicity it is assumed that such reduction of the total energy gain due to the shear stress reduction is approximately compensated by additional strain energy gain of NP that allows to ignore at a first approximation the influence of $-b$ -dislocations on LD emission.

For the sake of calculation simplicity within the present model, the influence of the stress field due to the EGBD pile-up near the triple junction on the LD emission may be ignored. Actually, the main fraction of the pile-up dislocations is concentrated in its head at the triple junction and is far enough from the LD emission point, and critical conditions for this emission are formed even with small (about 1 nm) displacement of the LD from point C.

The difference in elastic moduli of NP and surrounding grains will be also ignored herein, and the alloy material will be addressed as an elastically isotropic uniform medium. This will allow to ignore the effect of concentration of the applied stress τ on the NP edge while still remaining within the analytical model. Consideration of this effect would have required an excessively cumbersome finite element numerical model to be built which is absolutely unsuitable for our theoretical assessment analysis.

As an elastic model of NP, a dilatational inclusion in the form of a long parallelepiped with its longitudinal axis oriented perpendicular to the plane of Figure 1 will be used. Elastic fields of such inclusion are defined by its shape and inherent uniform 3D dilatation ε^* (see, for example, [29,30]). Dilatation ε^* is, in turn, defined by the misfit of the lattice constants of NP and surrounding alloy f , difference in their thermal expansion coefficients and difference in annealing temperature and mechanical test temperature.

3. Results

Calculate the energy characteristics of emission of the k -th LD from NP (Figure 1). Energy difference ΔW_k characterizing this process is expressed as follows:

$$\Delta W_k = E_k^{2b} + E_k^{NP-2b} + E_k^{B-2b} + E_k^{b-2b} + E_k^\tau, \quad (1)$$

where E_k^{2b} is the self energy of the k -th dipole of $\pm b$ -dislocations, E_k^{NP-2b} is the interaction energy be-

tween NP ABCD and the k -th dipole of $\pm b$ -dislocations, E_k^{B-2b} is the interaction energy between B -superdislocation in front of NP and the k -th dipole of $\pm b$ -dislocations, E_k^{b-2b} is the interaction energy between the k -th dipole of $\pm b$ -dislocations and wall EF consisting of $k-1$ climbing b -dislocations, E_k^τ is the interaction energy of the applied shear stress τ with the k -th dipole of $\pm b$ -dislocations.

The self energy E_k^{2b} is given by a known expression [31], while the interaction energies are calculated as the work spent to generate one defect in the stress field of another defect (group of defects) [32]. Finally, we obtain

$$E_k^{2b} = Db^2 \left(\ln \frac{p_k - r_c}{r_c} + 1 \right), \quad (2)$$

$$E_k^{NP-2b} = Db\varepsilon^*(1+\nu) \left(q \ln \left(1 + \frac{4c^2}{q^2} \right) - (q+p_k) \times \ln \left(1 + \frac{4c^2}{(q+p_k)^2} \right) - (q-p_k) \ln \left(1 + \frac{4c^2}{(q-p_k)^2} \right) + 4c \left(\arctan \frac{q}{2c} - \arctan \frac{q+p_k}{2c} - \arctan \frac{q-p_k}{2c} \right) \right), \quad (3)$$

$$E_k^{B-2b} = -\frac{DBb}{2} \left(\cos \alpha \ln \frac{h^2 + p_k^2 + 2hp_k \cos \alpha}{h^2} - \frac{2hp_k \sin^2 \alpha}{h^2 + p_k^2 + 2hp_k \cos \alpha} \right), \quad (4)$$

$$E_k^{b-2b} = 2Db^2 \sum_{i=1}^{k-1} \left(\ln \frac{(d-p_k)^2 + y_i^2}{d^2 + y_i^2} + \frac{2y_i^2 p_k (2d-p_k)}{[(d-p_k)^2 + y_i^2](d^2 + y_i^2)} \right), \quad (5)$$

$$E_k^\tau = -b\tau p_k \cos 2\alpha, \quad (6)$$

where $D = G/[2\pi(1-\nu)]$, G is the shear modulus, ν is the Poisson ratio, $r_c \approx b$ is the LD core radius, p_k is the distance covered by the emitted LD in the grain, $q = h \cos \alpha$, $c = h \sin \alpha$, $y_i = (i-1)a$, a is the crystal lattice constant in Al.

Using equations (1) to (6) to calculate the energy difference ΔW_k , find critical stress $\tau_c(k)$ which is the minimum stress required for intersection of the grain by the emitted LD (condition $p_k = d$). This stress is calculated from conditions [26] $\Delta W_k(p_k = p') = 0$, $\Delta W_k|_{p_k > p'} < 0$ and $\partial \Delta W_k / \partial p_k|_{p_k > p'} < 0$ where $p' = 1$ nm. It is associated with flow stress σ as follows: $\sigma = 2\tau_c(k) / \cos 2\alpha$. To assess the degree of plastic deformation induced by the emitted LDs, use the known relationship [26] $\varepsilon \approx kb/d$.

Using the estimates for flow stress σ and degree of plastic deformation ε , calculate dependences $\sigma(\varepsilon)$ for UFG Al-Cu-Zr alloy after HPT treatment, low-temperature annealing and additional small HPT deformation. Calculations were carried out for the following defect structure

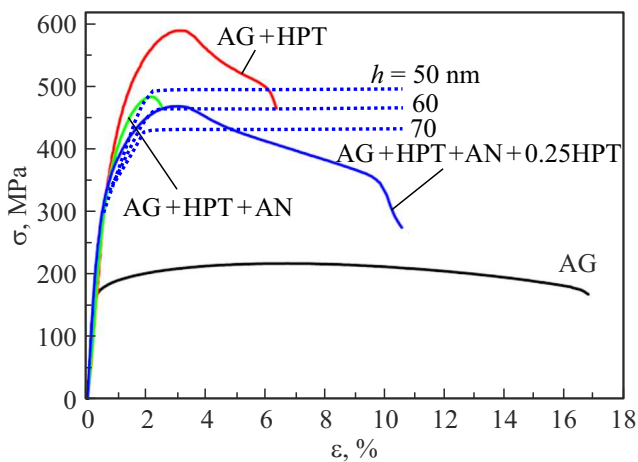


Figure 2. Theoretical dependences (dashed curves) of flow stress σ on plastic deformation ε for various NP sizes h . For comparison, experimental dependences $\sigma(\varepsilon)$ (solid curves) of Al-Cu-Zr UFG alloy at different thermomechanical treatment stages are shown [7].

parameters [33,34]: $G = 27$ GPa, $\nu = 0.33$, $a = 0.405$ nm, $b = a\sqrt{2}/2$, $b_{gb} = 0.1$ nm and $d \approx 300$ nm [7]. Angle $\alpha = 22^\circ$ was chosen as a mean angle between 0° and 45° that correspond to the maximum and minimum levels of the external shear stress τ . The number of EGBDs in front of the NP was assumed equal to $n = 18$ (this corresponds to the case of a single NP, described in theoretical study [35]). For dilatation eigenstrain of NP, a mean lattice misfit of aluminium matrix and Al_2Cu NP in two orthogonal orientations at interface $(110)_{\text{Al}_2\text{Cu}} \parallel (111)_{\text{Al}}$ [25] (see Section 2): $\varepsilon^* = f \approx (0.0123 + 0.0171)/2 = 0.0147$. In this case, the contribution of the thermal expansion coefficient difference was neglected due to its relative smallness (about

$$\begin{aligned} \Delta\alpha\Delta T &= (\alpha_{\text{Al}} - \alpha_{\text{Al}_2\text{Cu}})(T_{\text{AN}} - T_{\text{room}}) \\ &\approx (27 - 20) \cdot 10^{-6}(398 - 300) \approx 6.86 \cdot 10^{-4}, \end{aligned}$$

where α_{Al} and $\alpha_{\text{Al}_2\text{Cu}}$ are thermal expansion coefficients of Al and Al_2Cu , T_{AN} is the annealing temperature, T_{room} is room temperature).

Calculated dependences $\sigma(\varepsilon)$ (blue dashed curves) are shown in Figure 2 for different NP sizes h compared with experimental data [7] for UFG Al-Cu-Zr alloy in different states: aged alloy (black curve, AG), aged alloy after HPT treatment (red curve, AG+HPT), aged alloy after HPT treatment and additional low-temperature annealing at $T_{\text{AN}} = 125^\circ\text{C}$, 4 h (green curve, AG+HPT+AN), and aged alloy after HPT treatment, additional low-temperature annealing at $T_{\text{AN}} = 125^\circ\text{C}$, 4 h and small additional HPT (blue solid curve, AG+HPT+AN+0.25HPT). Figure 2 shows that theoretical dependences $\sigma(\varepsilon)$ at the initial LD emission stage demonstrate considerable growth of flow stress, and at the next stage after achievement of a certain flow stress level $\sigma = \sigma_{st}$, they attain the saturation and are

almost independent of the number of emitted LDs. This plastic deformation stage characterizes the increase in UFG alloy ductility after additional HPT deformation.

Comparison of the theoretical and experimental dependences has shown that the best match with the experiment is demonstrated by the theoretical curve corresponding to NP size $h = 60$ nm, which is aligned with the experimental data [7]. It should be noted that there is no flow stress growth restriction within this model. Therefore, the plastic deformation will be also continuously growing which is not consistent with reality. Thus, relying on the experimental data [7], a restriction for plastic deformation $\varepsilon = 11\%$ corresponding to the flow stress that has achieved saturation $\sigma = \sigma_{st}$ is artificially introduced herein. It should be also noted that the initial parts of theoretical curves do not coincide with the initial parts of experimental curves, because the theoretical curves describe only plastic deformation without taking into account the elastic component.

4. Conclusions

Thus, a theoretical model describing an increase in ductility of UFG Al-Cu-Zr alloy after HPT treatment, additional annealing and additional small HPT deformation has been developed. Within the suggested model, this increase in ductility is caused by the emission of lattice dislocations (LDs) by edges of faceted Al_2Cu nanoprecipitates (NPs) appearing on the grain boundaries (GBs) during thermomechanical treatment of the alloy. The flow stress and plastic deformation assessments demonstrate good agreement with the experimental data [7]. LD emission by NP edges ensures higher ductility compared with LD emission from GB triple junctions, since for NPs, the number of emitted LDs is not limited, unlike LD emission from the GB triple junctions when the number of emitted LDs is limited by the number of EGBDs in the pile-ups at the triple junctions. Moreover, in case of the UFG alloy subjected to additional low-temperature annealing and additional small HPT deformation, compared with the UFG alloy after low-temperature annealing, GBs have sufficient amounts of EGBDs to ensure Al_2Cu NP work as LD sources in multiple grains. All this ensures, in our opinion, high ductility of UFG Al-Cu-Zr alloy after additional HPT deformation.

Funding

This study was carried out under financial support of the Russian Science Foundation (grant No. 22-19-00292).

Conflict of interest

The authors declare that they have no conflict of interest.

References

- [1] K. Edalati, A. Bachmaier, V.A. Beloshenko, Y. Beygelzimer, V.D. Blank, W.J. Botta, K. Bryła, J. Čížek, S. Divinski, N.A. Enikeev, Y. Estrin, G. Faraji, R.B. Figueiredo, M. Fuji, T. Furuta, T. Grosdidier, J. Gubicza, A. Hohenwarter, Z. Horita, J. Huot, Y. Ikoma, M. Janeček, M. Kawasaki, P. Král, S. Kuramoto, T.G. Langdon, D.R. Leiva, V.I. Levitas, A. Mazilkin, M. Mito, H. Miyamoto, T. Nishizaki, R. Pippan, V.V. Popov, E.N. Popova, G. Purcek, O. Renk, Á. Révész, X. Sauvage, V. Sklenicka, W. Skrotzki, B.B. Straumal, S. Suwas, L.S. Toth, N. Tsuji, R.Z. Valiev, G. Wilde, M.J. Zehetbauer, X. Zhu. *Mater. Res. Lett.* **10**, 4, 163 (2022).
- [2] Y.T. Zhu, Y.H. Zhao, J.F. Bingert, T.D. Topping, P.L. Sun, X.Z. Liao, E.J. Lavernia. *Mater. Sci. Eng. A* **772**, 138706 (2020).
- [3] J. Gubicza. *Mater. Trans.* **60**, 1230 (2019).
- [4] X. Sauvage, G. Wilde, S. Divinski, Z. Horita, R. Valiev. *Mater. Sci. Eng. A* **540**, 1 (2012).
- [5] A.A. Nazarov. *Lett. Mater.* **8**, 3, 372 (2018).
- [6] I.A. Ovid'ko, R.Z. Valiev, Y.T. Zhu. *Progr. Mater. Sci.* **94**, 462 (2018).
- [7] T.S. Orlova, D.I. Sadykov, D.V. Danilov, N.A. Enikeev, M.Yu. Murashkin. *Mater. Lett.* **330**, 130490 (2021).
- [8] D. Raabe, D. Ponge, O. Dmitrieva, B. Sander. *Scr. Mater.* **60**, 1141 (2009).
- [9] K. Ming, X. Bi, J. Wang. *Int. J. Plast.* **100**, 177 (2018).
- [10] S.-H. Kim, H. Kim, N.J. Kim. *Nature* **518**, 77 (2015).
- [11] A.M. Mavlyutov, T.S. Orlova, E.Kh. Yapparova. *Tech. Phys. Lett.* **46**, 916 (2020).
- [12] V.D. Sitdikov, M.Yu. Murashkin, R.Z. Valiev. *J. Alloys Compd.* **735**, 1792 (2018).
- [13] Y. Nasedkina, X. Sauvage, E.V. Bobruk, M.Yu. Murashkin, R.Z. Valiev, N.A. Enikeev. *J. Alloys Compd.* **710**, 736 (2017).
- [14] W. Xu, X.C. Liu, K. Lu. *Acta Mater.* **152**, 138 (2018).
- [15] H. Jia, R. Bjørge, L. Cao, H. Song, K. Marthinsen, Y. Li. *Acta Mater.* **155**, 199 (2018).
- [16] L.F. Shuai, T.L. Huang, G.L. Wu, N. Hansen, X. Huang. *IOP Conf. Ser.: Mater. Sci. Eng.* **219**, 012038 (2017).
- [17] T.S. Orlova, D.I. Sadykov, M.Yu. Murashkin, N.A. Enikeev. *Phys. Solid State* **63**, 1744 (2021).
- [18] T.S. Orlova, D.I. Sadykov, D.V. Danilov, M.Y. Murashkin. *J. Alloy Compd.* **931**, 167540 (2023).
- [19] V. Borovikov, M.I. Mendeleev, A.H. King. *Scr. Mater.* **154**, 12 (2018).
- [20] S. Peng, Y. Wei, H. Gao. *PANS* **117**, 5204 (2020).
- [21] J.M. Howe, W.E. Benson, A. Garg, Y.C. Chang. *Mater. Sci. Forum* **189–190**, 255 (1995).
- [22] S.J. Wang, G. Liu, J. Wang, A. Misra. *Mater. Character.* **142**, 170 (2018).
- [23] G. Liu, M. Gong, D. Xie, J. Wang. *JOM* **71**, 4, 1200 (2019).
- [24] Q. Zhou, D.P. Hua, Y. Du, Y. Ren, W.W. Kuang, Q.S. Xia, V. Bhardwaj. *Int. J. Plast.* **120**, 115 (2019).
- [25] G. Liu, S. Wang, A. Misra, J. Wang. *Acta Mater.* **186**, 443 (2020).
- [26] N.V. Skiba, T.S. Orlova, M.Yu. Gutkin. *Phys. Solid State.* **62**, 2094 (2020).
- [27] K.N. Mikaelyan, M.Yu. Gutkin, E.N. Borodin, A.E. Romanov. *Int. J. Solid Struct.* **161**, 127 (2019).
- [28] A.M. Smirnov, S.A. Krasnitckii, M.Yu. Gutkin. *Acta Mater.* **186**, 494 (2020).
- [29] V.I. Vladimirov, M.Yu. Gutkin, S.P. Nikanorov, A.E. Romanov. *Mekhanika kompozitnykh materialov* **4**, 730 (1986). (in Russian).
- [30] K.L. Malyshev, M.Yu. Gutkin, A.E. Romanov, A.A. Sitnikova, L.M. Sorokin. *Sov. Phys. Solid State (USA)* **30**, 7, 1176 (1988).
- [31] M.Yu. Gutkin, I.A. Ovid'ko, N.V. Skiba. *Phil. Mag.* **88**, 1137 (2008).
- [32] T. Mura. In: *Advances in Material Research / Ed. H. Herman. Interscience, N.Y.* **3** (1968). P. 1.
- [33] J.P. Hirth, J. Lothe. *Theory of dislocations.* Wiley, N.Y. (1982).
- [34] C.J. Smithells, E.A. Brands. *Metals reference book.* Butterworths, London (1976).
- [35] M.Yu. Gutkin, N.V. Skiba, T.S. Orlova. *Mater. Phys. Mech.* **50**, 431 (2022).

Translated by E.Ilyinskaya